

Article ID: 1006-8775(2016) S1-0078-11

STUDY OF THE RELATIONSHIP BETWEEN IWC AND Z FOR NONSPHERICAL ICE PARTICLES AT MILLIMETER WAVELENGTH

WANG Jin-hu (王金虎)^{1,2}, GE Jun-xiang (葛俊祥)^{1,2}, WEI Ming (魏 鸣)^{1,2}, GU Song-shan (顾松山)²,
YANG Ze-xin (杨泽鑫)¹

(1. Jiangsu Key Laboratory of Meteorological Observation and Information Processing, Nanjing University of Information Science and Technology, Nanjing 210044 China; 2. Key Laboratory for Aerosol-Cloud-Precipitation of China Meteorological Administration, Nanjing University of Information Science and Technology, Nanjing 210044 China)

Abstract: Ice water content (IWC) plays important roles in weather and climate change. Determining the IWCs of cirrus clouds with millimeter-wavelength radar can be problematic due to influences of ice particle rotation on their backscattering cross sections. We here introduce models to describe the radiation patterns of six nonspherical particles of specific sizes. Simulations using HFSS software were applied to describe the differences resulting from different orientations and equivalent spheres. A double exponential function was used for fitting to describe the relationship between the particles' maximum sizes and backscattering cross sections. The backscattering cross sections of nonspherical ice particles were computed by the method of moment, and those of the equivalent spherical particles were computed by Lorenz-Mie theory for three different orientations: fixed, horizontal, and random. Assuming that a mixture of nonspherical ice particles follows the B-H mixing model, the size distribution of cirrus particles obeys the exponential distribution measured by NASA in 2007. By computing the IWCs of cirrus clouds, which follows the above mentioned B-H model and exponential distribution, the radar reflectivity factors of nonspherical ice particles and equivalent spheres at three different orientations can be computed. Subsequently, the IWC results can be acquired by inputting the radar reflectivity variables into the well-known IWC-Z formula. The analysis described here demonstrates that when using the radar reflectivity Z, the orientation must be considered in order to determine the IWC. Using equivalent sphere theory, the derived IWCs underestimate the actual IWCs. These results are important for accurately retrieving the microphysical parameters of cirrus clouds.

Key words: method of moment; ice particles; radar reflectivity factor; ice water content

CLC number: P426.5 **Document code:** A

doi: 10.16555/j.1006-8775.2016.S1.008

1 INTRODUCTION

Cirrus clouds play an important role in the global climate system through their effects on the radiative balance of the earth-atmosphere system (Zhang^[1]; Wang et al.^[2]; Wang et al.^[3]). Globally distributed cirrus clouds reflect or scatter short-wavelength radiation from the sun and absorb long-wavelength radiation from the atmosphere and the earth's surface.

Among cloud detection instruments, millimeter-wavelength radar has been widely used because it can detect the dynamical and structural properties of cirrus clouds (Fan et al.^[4]; Zhong et al.^[5]; Wang et al.^[6]). The macro- and micro-physical properties such as cloud height, cloud cover, and ice

water content (IWC) can be retrieved from the echoes of millimeter-wavelength radar. The IWC is an important micro-physical parameter that affects weather and climate change (Zhu et al.^[7]; Teng^[8]). There are many advantages of retrieving the IWC from radar echo signals; e.g., Atlas^[9] and Sauvageot^[10] determined the empirical relationships among radar reflectivity, effective cloud particle radius, and liquid water content (LWC). Liao and Sassen^[11] studied the relationship among radar reflectivity, LWC, and IWC, in the Ka- and W-bands. Sekelsky^[12] estimated particles' sizes and IWCs using the dual-wavelength ratio at 2.8 GHz, 33.12 GHz, and 94.92 GHz. Liu et al.^[13] investigated the IWCs,

Received 2015-10-21; Revised 2016-02-26; Accepted 2016-07-15

Foundation item: National Special Research Fund for Non-Profit (Meteorological) Section (GYHY201206038); Graduate Students' Scientific Research Innovation Program of Jiangsu Higher Education Institution of China (CXLX12_0500); National Nature Science Foundation of China (61372066); Jiangsu Innovation & Entrepreneurship Group Talents Plan

Biography: WANG Jin-hu, Ph.D. candidate, primarily undertaking research on atmospheric remote sensing.

Corresponding author: WANG Jin-hu, e-mail: goldtigerwang@nuist.edu.cn

LWCs, and phases of cloud particles with Ka-band radar data by referencing some empirical formulas.

Modeling an ice particle is very important to building an empirical formula between radar reflectivity factor and IWC. Some authors have studied this relationship assuming nonspherical particles to be spherical or ellipsoidal. For example, Wang et al. [14] assumed that the water content and number concentration of particles obey normal distributions and found a relationship between the attenuation coefficient K and the radar reflectivity factor Z by applying Mie theory at 3.2 mm. Matrosov and Heymsfield [15] assumed ice particles to be ellipsoidal and provided a relationship among their attenuation coefficients, IWCs, and Z values. However, by assuming nonspherical particles to be spherical or ellipsoidal, the computed reflectivity would underestimate the actual radar reflectivity (Tyynela et al. [16]; Hogan et al. [17]) when the radar vertically detects targets. Schneider and Stephens [18] studied the backscattering properties of hexagonal column, flake ice crystal, and dendritic snow crystal; they found that the relative error can reach 15% when nonspherical particles are equivalent to ellipsoidal particles; Petty and Huang [19] computed the scattering and extinction properties of aggregates and soft ice spheres by Rayleigh-Gans theory and found that the results from this equivalent theory pose a serious problems. Leinonen et al. [20] suggested that the ellipsoid particle approximation cannot describe the backscattering properties of ice particles when the radar wavelength is of the same order of magnitude as the particle size. Thus, the scattering results of equivalent sphere theory or equivalent ellipsoid theory would produce serious errors when compared to the actual backscattering properties of nonspherical particles. Based on the above discussion, the scattering properties of nonspherical ice particles are important for retrieving the LWCs or IWCs of clouds. However, the influence of particles' rotations on the radar reflectivity due to air motion is rarely mentioned, but the relevant literature indicates that the particles' orientations are dependent on ambient conditions (Zhang [21]; Wang et al. [22]; Wang et al. [23]). Thus, in this study, it was first assumed that the ice crystal was a column, a plate, hollow, a six-branch bullet rosette, an aggregate, or droxtal. Then it was assumed that the size distribution and mixing model obeyed an exponential distribution and the B-H model, respectively. The radar reflectivity factors of the six nonspherical particles were computed by the method of moment (MOM) for three different orientations: fixed, horizontal, and random. The scattering properties of equivalent spheres with the same volumes as the above-mentioned nonspherical particles were computed by Lorenz-Mie theory. Finally, we discuss how these different reflectivity

results affect the retrieved IWCs.

2 BASIC PRINCIPLE OF MOM

The electromagnetic field integral equation is the foundation of the method of moment (MOM). The electromagnetic field integral equations can be divided into surface integral equations (SIEs) and volume integral equations (VIEs). SIEs can be applied to homogeneous scattering media, and VIEs can be applied to inhomogeneous scattering media. SIEs can be used to compute the scattering properties of cirrus particles based on their characteristics.

According to the equivalence principle and uniqueness theorem of the electromagnetic field (Eom [24]) and combined with PMCHW (Chew et al. [25]), the SIEs can be derived as follows:

$$\bar{n}_1 \times \bar{E}^i = \bar{n}_1 \times \left\{ j\omega [\bar{A}_1 + \bar{A}_2] + [\nabla\Phi_1 + \nabla\Phi_2] + \nabla \times \left[\frac{\bar{F}_1}{\epsilon_1} + \frac{\bar{F}_2}{\epsilon_2} \right] \right\} \quad (1)$$

and

$$\bar{n}_1 \times \bar{H}^i = \bar{n}_1 \times \left\{ j\omega [\bar{F}_1 + \bar{F}_2] + [\nabla\Psi_1 + \nabla\Psi_2] - \nabla \times \left[\frac{\bar{A}_1}{\mu_1} + \frac{\bar{A}_2}{\mu_2} \right] \right\} \quad (2)$$

where \bar{E}^i is the incident electric field and \bar{H}^i is the incident magnetic field. \bar{A} , \bar{F} , Φ , and Ψ are the magnetic vector potential, electric vector potential, electric scalar potential, and magnetic scalar potential, respectively.

The electric and magnetic current sources can be expanded as follows according to the RWG basis function (Rao [26]):

$$\bar{J} = \sum_{m=1}^n L_m \bar{f}_m \quad (3)$$

and

$$\bar{M} = \sum_{m=1}^n M_m \bar{f}_m \quad (4)$$

where

$$\bar{f}_n(r) = \begin{cases} \frac{l_n}{2A_n^+} \bar{\rho}_n^+ & r \in T_n^+ \\ \frac{l_n}{2A_n^-} \bar{\rho}_n^- & r \in T_n^- \\ 0 & \text{others} \end{cases} \quad (5)$$

and l_n is the length of the inner edge of a pair of triangles, T_n^+ and T_n^- are two associated triangles, A_n^+ and A_n^- are the area of the triangles, and $\bar{\rho}_n^+$ and $\bar{\rho}_n^-$ are position vectors that point outside and inside of the vertex, respectively.

Based on Galerkin's method (Nie and Fang [27]), the weighting function, which comes from the RWG

basis function weight, combined with the field integral equation, Eqs. (1) and (2), we can obtain the following formulas:

$$\langle \bar{E}^i, \bar{f}_m \rangle = \langle j\omega[\bar{A}_1 + \bar{A}_2], \bar{f}_m \rangle + \langle [\nabla\Phi_1 + \nabla\Phi_2], \bar{f}_m \rangle + \left\langle \nabla \times \left[\frac{\bar{F}_1}{\epsilon_1} + \frac{\bar{F}_2}{\epsilon_2} \right], \bar{f}_m \right\rangle \quad (6)$$

and

$$\langle \bar{H}^i, \bar{f}_m \rangle = \langle j\omega[\bar{F}_1 + \bar{F}_2], \bar{f}_m \rangle + \langle [\nabla\Psi_1 + \nabla\Psi_2], \bar{f}_m \rangle - \left\langle \nabla \times \left[\frac{\bar{A}_1}{\mu_1} + \frac{\bar{A}_2}{\mu_2} \right], \bar{f}_m \right\rangle \quad (7)$$

The matrix form of Eqs. (6) and (7) can be derived from some calculation and approximation as

$$\begin{bmatrix} [X_{mn}] & [C_{mn}] \\ [D_{mn}] & [Y_{mn}] \end{bmatrix} \begin{bmatrix} [I_n] \\ [M_n] \end{bmatrix} = \begin{bmatrix} [E_n] \\ [H_n] \end{bmatrix} \quad (8)$$

The specific expressions of Eq. (8) can be found in the relevant literature (Nie and Fang^[28]) and Eq. (8) can be simplified to:

$$\bar{Z} \times \bar{I} = \bar{V} \quad (9)$$

where \bar{Z} is the impedance matrix, \bar{I} is the electric and magnetic current coefficient, and \bar{V} is the electric and magnetic field excitation matrix.

To determine the electric and magnetic current coefficient \bar{I} , the impedance matrix \bar{Z} must first be obtained, as it determines the interaction between the different edges. However, the integral value of Green's function tends to approach infinity when the source point coincides with the field point, and the infinite value can cause the diagonal elements of the impedance matrix to become infinite in amplitude. To process the impedance matrix singularity, the "centroid cutting method" is presented in this paper (Makarov^[29]). The electric and magnetic current coefficient \bar{I} can be obtained by the matrix's left divide operation after acquiring the impedance matrix.

The dipole radiation field can be computed using the dipole model method, which implies that the radiation field, located at the position vector \bar{r} of the infinitesimal electric dipole at the origin, can be expressed as follows:

$$\bar{H}_e = \frac{j\mathbf{k}}{4\pi} (\bar{m} \times \bar{r}) C e^{-jkr}, C = \frac{1}{r^2} \left(1 + \frac{1}{jkr} \right) \quad (10)$$

and

$$\bar{E}_e = \frac{\eta}{4\pi} [(\bar{Q} - \bar{m}) \left(\frac{j\mathbf{k}}{r} + C \right) + 2\bar{Q}C] e^{-jkr}, \bar{Q} = \frac{(\bar{r} \cdot \bar{m}) \bar{r}}{r^2} \quad (11)$$

Similarly, the radiation field located at the position vector \bar{r} of the infinitesimal magnetic dipole at the origin can be expressed as follows:

$$\bar{E}_m = -\frac{j\mathbf{k}}{4\pi} (\bar{p} \times \bar{r}) C e^{-jkr}, C = \frac{1}{r^2} \left(1 + \frac{1}{jkr} \right) \quad (12)$$

and

$$\bar{H}_m = \frac{1}{4\pi\eta} [(\bar{Q} - \bar{p}) \left(\frac{j\mathbf{k}}{r} + C \right) + 2\bar{Q}C] e^{-jkr}, \bar{Q} = \frac{(\bar{r} \cdot \bar{p}) \bar{r}}{r^2} \quad (13)$$

The radar cross-section under far-field conditions can be expressed as

$$\sigma = \lim_{R \rightarrow \infty} 4\pi R^2 \frac{|\bar{E}^s|^2}{|\bar{E}^i|^2} = \lim_{R \rightarrow \infty} 4\pi R^2 \frac{|\bar{H}^s|^2}{|\bar{H}^i|^2} \quad (14)$$

where $\bar{E}^s = \bar{E}_e + \bar{E}_m$ and $\bar{H}^s = \bar{H}_e + \bar{H}_m$.

3 SCATTERING PROPERTIES OF NONSPHERICAL ICE PARTICLES

Ice particles exhibit various sizes and characteristics at different altitudes (Gallagher et al.^[30]). The characteristics of column, plate, hollow, rosette, aggregate, and droxtal ice crystals are considered in this paper and are shown in Table 1 (Gang^[31]).

The complex dielectric constant of an ice particle is $\epsilon = 3.13 - j0.011$ (Aydin and Walsh^[32]). The wavelength of the incident electromagnetic wave is 3.2 mm. The difference in the scattering properties at different orientations and the errors of equivalent spheres can be simulated by the High-Frequency Structure Simulator (HFSS). The specific sizes of the six types of nonspherical ice particles can be defined as follows, where the sizes have the aspect ratio relationships listed in Table 1 (units: μm):

① Column: $L = 800, a = 98.4293$; ② Plate:

$L = 42.5872, a = 400$; ③ Hollow:

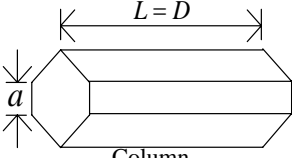
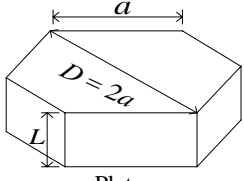
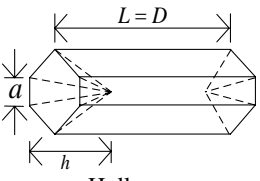
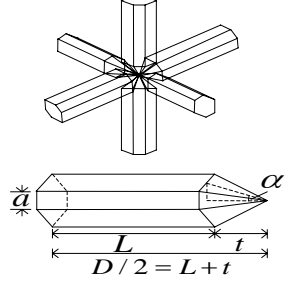
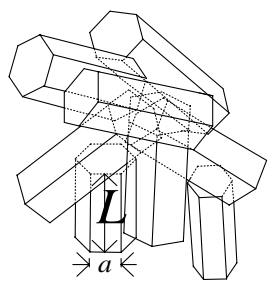
$a = 98.4293, h = 200$; ④ Six-branch bullet rosette:

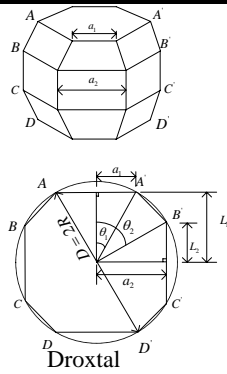
$L = 800, a = 104.6739, t = 170.4883$; ⑤

Aggregate: $L_1 = 800, a_1 = 232.8, L_2 = 802, a_2 = 259.046, L_3 = 803, a_3 = 288.277, L_4 = 804, a_4 = 306.324, L_5 = 805, a_5 = 296.24, L_6 = 806, a_6 = 283.712, L_7 = 807, a_7 = 268.731, L_8 = 808, a_8 = 252.096$; ⑥

Droxtal: $R = 400$, $a_1 = 214.0359$, $r_{hollow} = 158.8206$, $r_{bullet\ rosette} = 326.9103$,
 $L_2 = 124.8676$, $a_2 = 380.0106$, $L_1 = 337.9181$. $r_{aggregate} = 687.9868$, and $r_{droxtal} = 359.0593$. The
 The radii of the equivalent spheres of the above six nonspherical particles (units: μm) are
 $r_{column} = 168.7721$, $r_{plate} = 161.6792$,

Table 1. Six characteristics and corresponding parameters of cirrus cloud.

Geometrical shape	Aspect ratio	Volume
 <p>Column</p>	$\begin{cases} a = 0.35L & (L < 100\mu\text{m}) \\ a = 3.48L^{0.5} & (L \geq 100\mu\text{m}) \end{cases}$	$V = \frac{3\sqrt{3}}{2}a^2L$
 <p>Plate</p>	$\begin{cases} L = 2a & (a \leq 2\mu\text{m}) \\ L = 2.4883a^{0.474} & (a \geq 5\mu\text{m}) \\ L = 2 + ((2.4883a^{0.474} - 2) / 4) \cdot (a - 1) & (2\mu\text{m} < a < 5\mu\text{m}) \end{cases}$	$V = \frac{3\sqrt{3}}{2}a^2L$
 <p>Hollow</p>	$\begin{cases} a = 0.35L & (L < 100\mu\text{m}) \\ a = 3.48L^{0.5} & (L \geq 100\mu\text{m}) \\ h = 0.25L \end{cases}$	$V = \frac{3\sqrt{3}}{2}a^2L - \sqrt{3}a^2h$
 <p>6-branch Bullet Rosette</p>	$\begin{cases} a = 1.552L^{0.63} \\ t = \frac{\sqrt{3}a}{2 \tan \alpha} \quad \alpha = 28^\circ \end{cases}$	$V = 3\sqrt{3}a^2 \cdot (3L+t)$
 <p>Aggregate</p>	$\begin{aligned} a_1 &= 0.291L_1 & a_2 &= 0.323L_2 \\ a_3 &= 0.359L_3 & a_4 &= 0.381L_4 \\ a_5 &= 0.368L_5 & a_6 &= 0.352L_6 \\ a_7 &= 0.333L_7 & a_8 &= 0.312L_8 \\ D &= 7.297L_{\min} \end{aligned}$	$V = \sum_{i=1}^8 \frac{3\sqrt{3}}{2}a_i^2L_i$



$$D = 2R$$

$$a_1 = R \sin \theta_1 \quad a_2 = R \sin \theta_2$$

$$L_1 = R \cos \theta_1 \quad L_2 = R \cos \theta_2$$

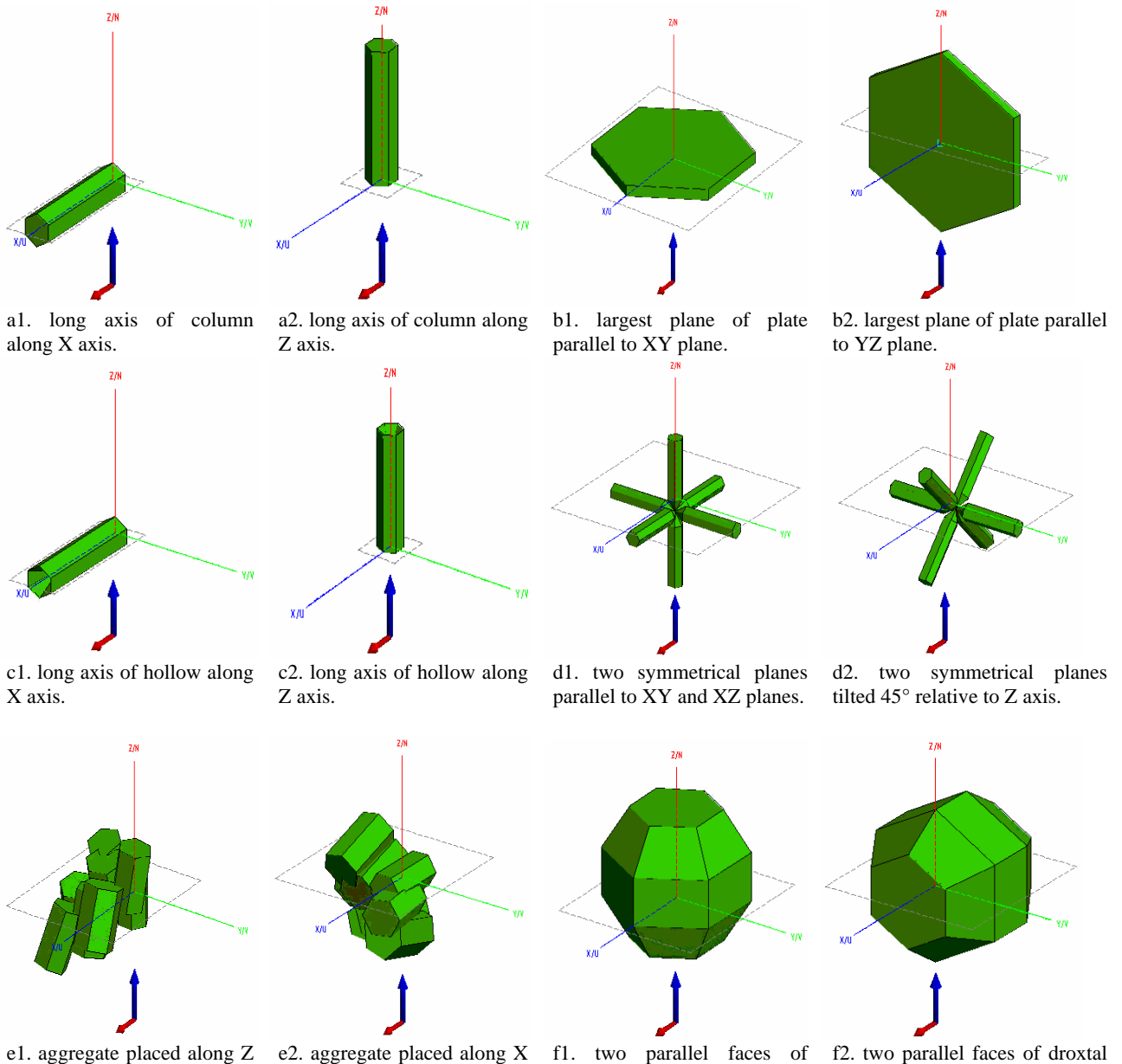
$$\theta_1 = 32.35^\circ \quad \theta_2 = 71.81^\circ$$

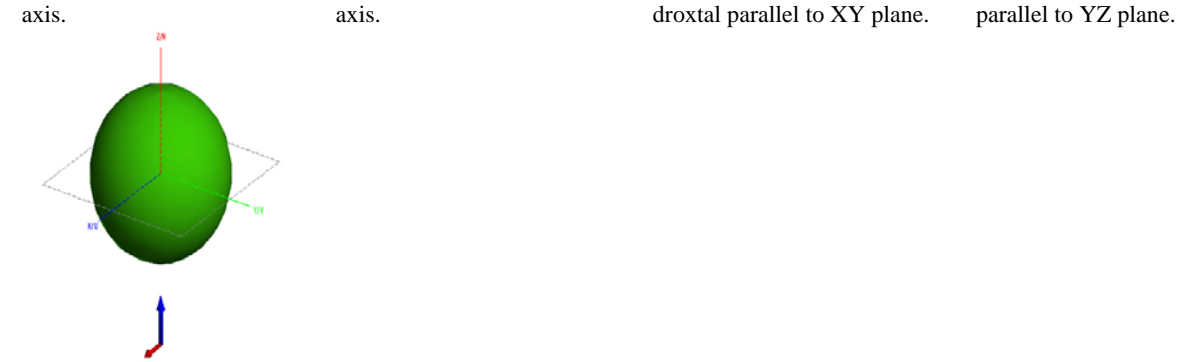
$$V = [(L_1 + 2L_2 + h) \cdot$$

$$a_2^2 - ha_1^2] \sqrt{3}$$

$$h = \frac{a_1(L_1 - L_2)}{a_2 - a_1}$$

Figure 1 shows the interaction between ice particles and incident electromagnetic wave. Note that the blue arrow along the positive Z axis denotes the incident direction of electromagnetic wave and that the red arrow along the positive X axis denotes the polarization direction of electric field. The influence on the scattering properties of spherical particles at different orientations will not be considered due to its symmetry. The simulated radiation patterns are shown in Fig. 2.





g. center of sphere located at origin of coordinate system.

Figure 1. Interaction between incident electromagnetic wave and particle based on HFSS.

Figure 2 shows the radiation patterns of particles that change due to the particles' orientations. However, the differences between the different positions may not be obvious due to small particles. No matter whether a particle is nonspherical or spherical, its side-scattering energy should be less than its forward-scattering energy (interaction point value of the radiation pattern with the positive Z-axis) and the backward scattering energy (interaction point value of the radiation pattern with the negative Z-axis). Moreover, the forward-scattering energy should be greater than the backward-scattering energy. The backscattering cross-sections of the six nonspherical ice particles and their corresponding equivalent spherical particles are shown in Table 2.

Table 2 shows that the backscattering cross-sections of fixed particles are larger than those of rotated particles. The main reason for this is that the cross-sectional area of the interaction between a fixed particle and the polarization direction of the electric field is larger than the interaction between a rotated particle and the polarization direction of the electric field. Therefore, the induced current of a fixed particle is larger than that of a rotating particle. Therefore, when radar detects nonspherical cirrus ice particles, the RCSs of the particles will change because of air movement, which is commonly referred to as "echo fluctuation" (Zhang et al.^[33]). The results also show that there are some deviations between the RCSs of nonspherical particles and those of the

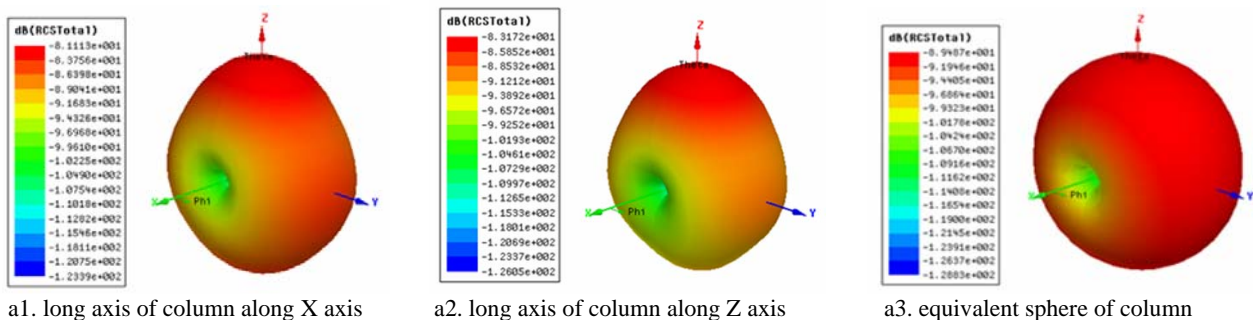
equivalent spherical particles. Thus, to accurately model the actual detection conditions when using the equivalent sphere theory, an RCS correction must be introduced. When the IWC of a cirrus cloud maintains a fixed value, the backscattering cross-section of the cloud will change due to particle movement. Subsequently, uncertainties appear in the relationship between radar reflectivity and IWC; thus, the phenomenon of ice particle rotation must be considered when studying the scattering properties of ensembles of particles.

4 IWC-Z RELATIONSHIPS OF ENSEMBLES OF PARTICLES

Section 3 described the scattering characteristics of nonspherical particles at different positions and the errors associated with the equivalent sphere theory. However, meteorological targets are not just single particles, but ensembles of particles. Therefore, to more realistically derive the radar reflectivity factors of ensembles of particles with different orientations and equivalent sphere theory, we applied the exponential distribution of ice particles measured by NASA in 2007 (Tian et al.^[34]):

$$N(D) = 2.18 \times 10^6 \cdot e^{-4.641D} \quad (15)$$

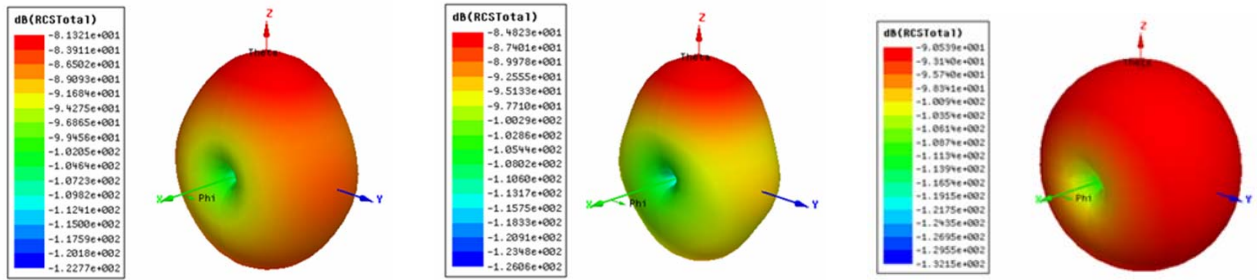
where the particles' diameter D ranges from 0.163 mm to 2.8 mm, and the ice particle density is $0.917 \text{ g}\cdot\text{m}^{-3}$.



a1. long axis of column along X axis

a2. long axis of column along Z axis

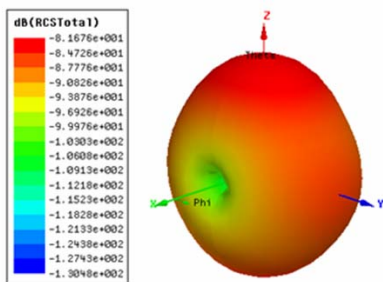
a3. equivalent sphere of column



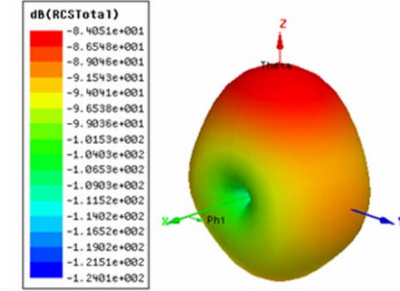
b1. largest plane of plate parallel to XY plane

b2. largest plane of plate parallel to YZ plane

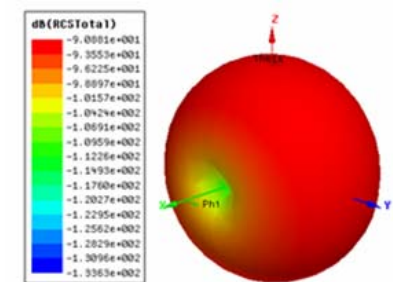
b3. equivalent sphere of plate



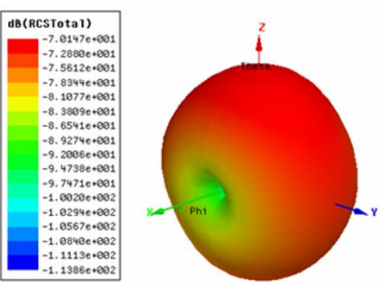
c1. long axis of hollow along X axis



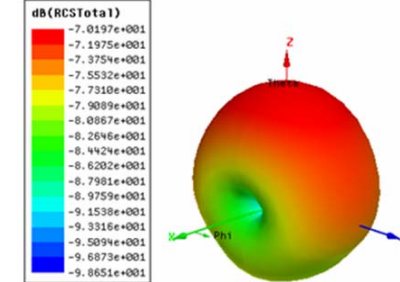
c2. long axis of hollow along Z axis



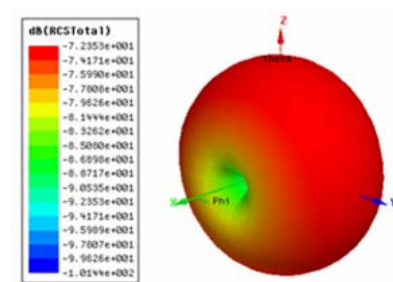
c3. equivalent sphere of hollow



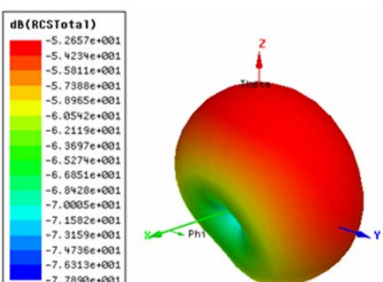
d1. two symmetrical planes parallel to XY and XZ planes



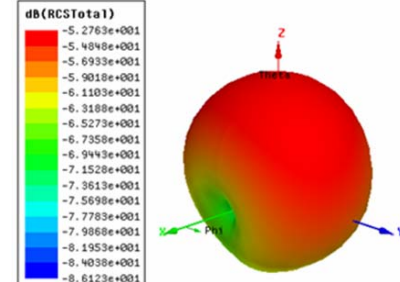
d2. two symmetrical planes titled 45° relative to Z axis



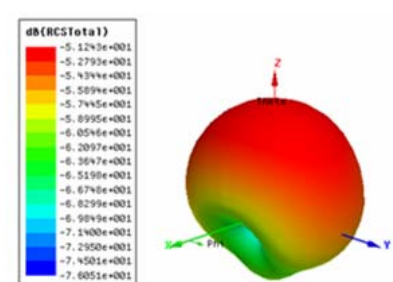
d3. equivalent sphere of bullet rosette



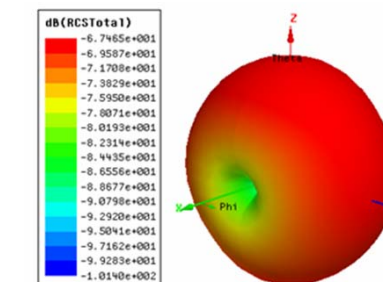
e1. aggregate placed along Z axis



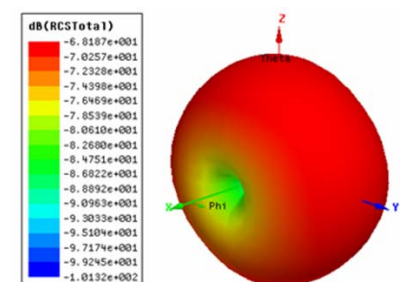
e2. aggregate placed along X axis



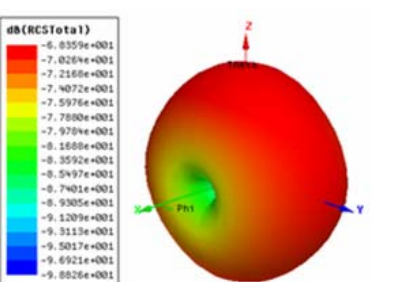
e3. equivalent sphere of aggregate



f1. two parallel faces of droxtal parallel to XY plane



f2. two parallel faces of droxtal parallel to YZ plane



f3. equivalent sphere of droxtal

Figure 2. Radiation patterns of different ice particles.

Table 2. RCSs of nonspherical particles and equivalent spheres (units: dBm²).

Geometrical shape	RCS of fixed particle	RCS of rotated particle	RCS of equivalent sphere
Column	-84.8451	-92.7715	-91.8502
Plate	-85.6304	-94.0527	-93.0677
Hollow	-85.8341	-92.8908	-93.4829
Bullet Rosette	-75.7696	-80.1834	-74.7109
Aggregate	-60.5762	-69.1474	-61.0496
Droxtal	-69.8613	-70.0769	-70.7171

Assuming the ice particles obey the B-H mixing model, which consists of 100% droxtals when $D < 0.06$ mm; 15% bullet rosettes, 50% columns, and 35% plates when 0.06 mm $< D < 1$ mm; 45% hollow columns, 45% columns, and 10% aggregates when 1 mm $< D < 2.5$ mm; and 97% bullet rosettes and 3% aggregates when $D > 2.5$ mm (Baum et al.^[35]). According to the particle size distribution and B-H mixing model, the IWC was computed to be 0.0737 g·m⁻³. However, when the IWC remains unchanged, there is the question of the differences between the radar reflectivity factors in the three different cases (fixed, horizontal, and random orientation), and how the differences in the radar reflectivity factors affect nonspherical ice particles and their equivalent spheres.

Before answering these questions, the relationships between the maximum sizes of the six nonspherical ice particles and their backscattering cross-sections were computed by the MOM. Notice that the nonspherical ice particle backscattering cross-section units are m² in the electromagnetic field. However, the units of radar reflectivity are mm⁶·m⁻³ in the meteorological field. The corresponding relationship between backscattering cross-section σ and the radar reflectivity factor Z can be expressed as follows (Zhang^[21]).

$$Z = \frac{\lambda^4}{\pi^5} \left| \frac{m^2 - 1}{m^2 + 2} \right|^{-2} \cdot \int_0^{D_{\max}} N(D) \sigma(D) dD \quad (16)$$

where λ is the incident electromagnetic wavelength, m is the complex refractive index of the ice particle, D_{\max} is the maximum particle size, $N(D)$ is the size distribution, and $\sigma(D)$ is the backscattering cross-section.

The following four situations were considered in studying how the orientation and equivalent sphere theory influence radar reflectivity:

I. For a mixture with fixed orientation (the fixed placement of the particle just as in Figs. 1(a1), 1(b1), 1(c1), 1(d1), 1(e1), and 1(f1)), the relationships between the backscattering cross-sections of the particles and the particles' sizes, as computed by the MOM, are as follows:

$$\begin{cases} \sigma_{\text{column}} = -108.3e^{-0.01264x} - 99.93e^{-0.000137x} \\ \sigma_{\text{plate}} = -113.4e^{-0.009731x} - 102.4e^{-0.0001638x} \\ \sigma_{\text{hollow}} = -116.2e^{-0.01272x} - 101.1e^{-0.0001345x} \\ \sigma_{\text{bullet rosette}} = -43.5e^{-0.00154x} - 86.37e^{-8.434 \times 10^{-5}x} \\ \sigma_{\text{aggregate}} = -60.91e^{-0.001536x} - 94.16e^{-7.242 \times 10^{-5}x} \\ \sigma_{\text{droxtal}} = -111.6e^{-0.01001x} - 88.44e^{-0.0001755x} \end{cases} \quad (17)$$

where the units of σ are dBm², and the units of x are μm .

II. For a mixture in a horizontal orientation (the average results of nonspherical particles rotating in the XY plane), the relationships between the backscattering cross-sections of the particles and the particles' sizes, as computed by the MOM, are as follows:

$$\begin{cases} \sigma_{\text{column}} = -110.2e^{-0.01292x} - 101.5e^{-0.0001308x} \\ \sigma_{\text{plate}} = -113.8e^{-0.01159x} - 104e^{-0.0001689x} \\ \sigma_{\text{hollow}} = -79.44e^{-0.007124x} - 98.95e^{-0.0001169x} \\ \sigma_{\text{bullet rosette}} = -69.82e^{-0.003228x} - 92.63e^{-9.829 \times 10^{-5}x} \\ \sigma_{\text{aggregate}} = -63.08e^{-0.002008x} - 98.48e^{-8.308 \times 10^{-5}x} \\ \sigma_{\text{droxtal}} = -113.2e^{-0.009981x} - 90.31e^{-0.0001678x} \end{cases} \quad (18)$$

where the units of σ are dBm², and the units of x are μm .

III. For a mixture with random orientations (the average results of nonspherical particles randomly rotated within the XYZ coordinate system), the relationships between the particle backscattering cross-sections and the particles' sizes, as computed by MOM, are as follows:

$$\begin{cases} \sigma_{\text{column}} = -74.94e^{-0.006116x} - 96.57e^{-0.0001065x} \\ \sigma_{\text{plate}} = -84.54e^{-0.007245x} - 100.3e^{-0.0001479x} \\ \sigma_{\text{hollow}} = -83.92e^{-0.006959x} - 98.63e^{-0.0001069x} \\ \sigma_{\text{bullet rosette}} = -72.07e^{-0.003134x} - 91.97e^{-9.215 \times 10^{-5}x} \\ \sigma_{\text{aggregate}} = -62.23e^{-0.001843x} - 95.48e^{-7.882 \times 10^{-5}x} \\ \sigma_{\text{droxtal}} = -87.66e^{-0.005344x} - 80.52e^{-0.0001393x} \end{cases} \quad (19)$$

where the units of σ are dBm², and the units of x are μm .

IV. For the spherical equivalent mixture (the volume of a spherical particle is equal to the volume of a nonspherical particle), the relationship between the particle's backscattering cross-section and the particle size, as computed by the MOM, is as follows:

$$\sigma_{sphere} = -108.9e^{-0.007561x} - 79.94e^{-0.0001561x} \quad (20)$$

where the units of σ are dBm², and the units of x are μm .

By combining the B-H mixing model with Eqs.(17)-(20), the radar reflectivity factors for the fixed, horizontal, random, and equivalent sphere orientations were computed to be 0.7975 mm⁶·m⁻³ (-0.9829 dBz), 0.5968 mm⁶·m⁻³ (-2.2416 dBz), 0.3881 mm⁶·m⁻³ (-4.1100 dBz), and 0.0376 mm⁶·m⁻³ (-14.2473 dBz), respectively. Obviously, the backscattering value is maximized in the fixed orientation, followed by the values in the horizontal and random orientations, and its value is minimized in the equivalent sphere orientation.

The IWCs can be retrieved by the relationship between IWC and Z ($IWC = aZ^b$). The proposed formulas are listed in Table 3.

Applying the backscattering cross sections of fixed, horizontal, random, and equivalent sphere orientations to the exponential relationships of Table 3, the different IWC values are as shown in Fig. 3.

Figure 3 shows the results obtained from the

different formulas, which are indicated by using different symbols. The blue dotted line indicates the actual value. For the equivalent sphere theory, the result computed by Matrosov’s formula (0.0636 g·m⁻³) is close to the actual value (0.0737 g·m⁻³), with a relative error of 13.7%. For the random orientation, the result computed by Brown’s formula (0.0759 g·m⁻³) is close to the actual value (0.0737 g·m⁻³), with a relative error of 2.99%. For the horizontal orientation, the result computed by Liu and Illingworth’s formula (0.0715 g·m⁻³) is close to the actual value (0.0737 g·m⁻³), with a relative error of 2.99%. For the fixed orientation, the result computed by Seo and Liu’s formula (0.0652 g·m⁻³) is close to the actual value (0.0737 g·m⁻³), with a relative error of 11.53%. Clearly, no matter which formula was used, the IWC value derived from the radar reflectivity by equivalent sphere theory is smaller than the actual value. Thus, the orientation must be considered when calculating the IWC, and the result obtained by equivalent sphere theory underestimates the actual IWC value.

Table 3. Empirical coefficients of IWC-Z formula.

authors	a	b
Liu and Illingworth ^[36]	0.097	0.59
Mace et al. ^[37]	0.1037	0.516
Seo and Liu ^[38]	0.078	0.79
Atlas ^[9]	0.064	0.58
Brown et al. ^[39]	0.153	0.74
Aydin and Tang ^[40]	0.104	0.483
Matrosov and Heymisfield ^[15]	0.086	0.092

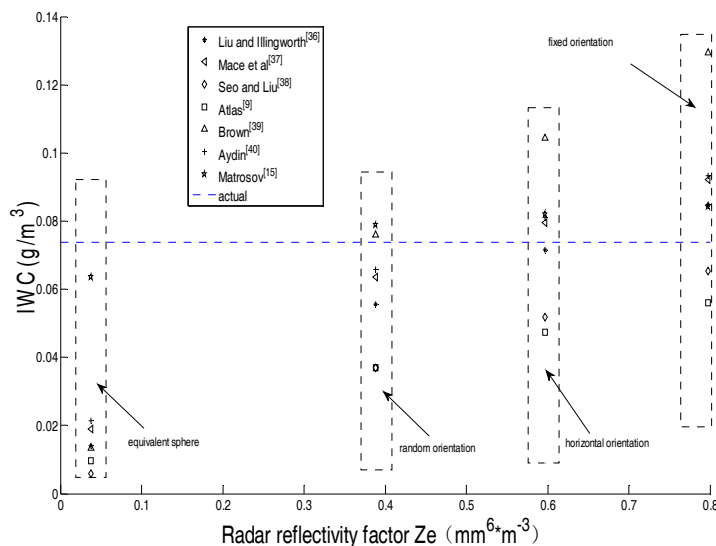


Figure 3. IWC values retrieved by radar reflectivity factors using different formulas.

5 CONCLUSIONS

The scattering properties of nonspherical and equivalent spherical particles were computed by

MOM and Lorenz-Mie theory, respectively. The radiation patterns of these particles at three orientations can be determined by HFSS software by fitting the particle backscattering cross-sections and sizes to double exponential functions. By combining the actual measured size distribution with the B-H

mixing model, the IWC value can be computed. Subsequently, the differences between the backscattering cross-sections of different orientations and of the equivalent sphere can be determined. The results showed that the minimum value was derived from the equivalent spherical model and that the maximum value was derived from the fixed orientation model. Comparing the IWC values obtained from different formulas indicated that the values determined by using equivalent spheres were all smaller than the actual value. Thus, different formulas should be used to calculate the IWCs for different orientations and equivalent spheres, namely, the equivalent spherical model, random orientation, horizontal orientation, and fixed orientation should utilize Matrosov's formula, Brown's formula, Liu and Illingworth's formula, and Seo-Liu's formula, respectively. In summary, the particles' orientations must be considered when determining IWCs using radar reflectivity factors, and a correction must be applied to the equivalent spherical model.

Acknowledgement: The authors thank the NASA Radiation Sciences Program for the use of their data.

REFERENCES:

- [1] ZHANG Lin. Study on the radiative transmission and scattering properties of cirrus clouds [D]. Master's thesis, Xidian University, 2010:1-2. (in Chinese)
- [2] WANG Jin-hu, GE Jun-xiang, WEI Ming, et al. Research progress on theoretical computation and experimental measurement of scattering properties of ice particles [J]. *Comput Tech Automat*, 2013, 32 (3): 128-131 (in Chinese).
- [3] WANG Jin-hu, GE Jun-xiang, WEI Ming, et al. Analysis of backscattering property of Cirrus cloud based on HFSS [C]. The 30th China Meteorological Conference, Nanjing, China, 2013: 1-8 (in Chinese).
- [4] FAN Ya-wen, HUANG Xing-you, LI Feng. A case study on cloud measurement with a 35 GHz millimeter-wave cloud radar [J]. *Trans Atmos Sci*, 2013, 36 (5): 554-559 (in Chinese).
- [5] ZHONG Ling-zhi, LIU Li-ping, GE Run-sheng. Characteristics about the millimeter-wavelength radar and its status and prospect in and abroad [J]. *Adv Earth Sci*, 2009, 24 (4): 383-391 (in Chinese).
- [6] WANG Jin-hu, GE Jun-xiang, WEI Ming, et al. Error analysis of equivalent sphere theory for calculating the scattering properties of ice crystals at millimeter wavelength [J]. *J Henan Normal Univ (Nat Sci Ed)*, 2014, 42 (5): 40-44 (in Chinese).
- [7] ZHU Ya-ping, CHEN Zhou-jie, LIU Jian-Wen, et al. A technique of analyzing multi-spectral clouds for southeast coast of china based on daytime satellite imagery [J]. *J Trop Meteorol*, 2014, 30 (4): 612-622 (in Chinese).
- [8] TENG Xu. A study of relationships amongst Z-LWC, Z-IWC at millimeter wavelength [C]. The 30th China Meteorological Conference, Nanjing, China, 2013: 1-6 (in Chinese).
- [9] ATLAS D. The estimation of cloud parameters by radar [J]. *J Meteorol*, 1954, 11: 309-317.
- [10] SAUVAGEOT H, OMAR J. Radar reflectivity of cumulus clouds [J]. *J Atmos Oceanic Tech*, 1987, 4: 264-272
- [11] LIAO L, SASSEN K. Theoretical investigation of the relationship between ice mass content and Ka-band radar reflectivity facote [C]. 11th Int. Conference on Cloud Physics and Precipitation, Montreal, Amer Meteorol Soc, 1992: 1 005-1 008.
- [12] SEKELSKY S M, MCINTOSH R E. Cloud observation with a polarimetric 33GHz and 95 GHz [J]. *Meteorol Atmos Phys*, 1996, 59: 123-140.
- [13] LIU Li-ping, ZHONG Ling-zhi, JIANG Yuan et al. Cloud radar and its field experiments in China [J]. *Meteorol Sci Tech*, 2009, 37 (5): 567-572 (in Chinese).
- [14] WANG Zhen-hui, TENG Xu, JI Lei, et al. A study of the relationship between the attenuation coefficient and radar reflectivity factor for spherical particles in clouds at millimeter wavelengths [J]. *Acta Meteorol Sinica*, 2011, 69 (6): 1 020-1 028 (in Chinese).
- [15] MATROSOV S Y, HEYMSFIELD A J. Estimating ice content and extinction in precipitating cloud systems from CloudSat radar measurements [J]. *J Geophys Res: Atmospheres*, 2008, 113: D00A05
- [16] TYYNELA J, LEINONEN J, MOISSEEV D, et al. Radar backscattering from snowflakes: comparison of fractal, aggregate, and soft spheroid models [J]. *J Atmos Oceanic Tech*, 2011, 28 (11): 1 365-1 372.
- [17] HOGAN R J, TIAN L, BROWN P R A, et al. Radar scattering from ice aggregates using the horizontally aligned oblate spheroid approximation [J]. *Appl Meteorol Climatol Mag*, 2012, 51 (3): 655-671.
- [18] SCHNEIDER T L, STEPHENS G L. Theoretical aspects of modeling backscattering by cirrus ice particles at millimeter wavelengths [J]. *J Atmos Sci*, 1995, 52 (23): 4 367-4 385.
- [19] PETTY G W, HUANG W M. Microwave backscatter and extinction by soft ice spheres and complex snow aggregates [J]. *J Atmos Sci*, 2010, 67 (3): 769-787.
- [20] LEINONEN J, KNEIFEL S, MOISSEEV D, et al. Evidence of nonspherical behavior in millimeter-wave length radar observations of snowfall [J]. *J Geophys Res: Atmospheres*, 2012, 117: 1-10.
- [21] ZHANG Z B. Computation of the scattering properties of nonspherical ice crystals [D]. Texas: Texas A & M University, 2004: 57-78.
- [22] WANG Jin-hu, Ge Jun-xiang, WEI Ming. Theoretical study on single-scattering properties of ice particles of different orientation at 94 GHz [J]. *Prog Electromag Res M*, 2014, 36: 39-46.
- [23] WANG Jin-hu, Ge Jun-xiang, WEI Ming. The influence of aspect ratio and orientation to scattering properties of ellipsoid ice particles [J]. *TELKOMNIKA Indonesian J Electr Engin*, 2014, 12 (11): 7 543-7 548.
- [24] EOM H J. Electromagnetic wave theory for boundary-value problems [M]. Berlin: Springer, 2002: 125-143.
- [25] CHEW W C, JIN J M, MICHELSEN E, et al. Song, eds. *Fast and Efficient Algorithms in Computational Electromagnetics* [M]. Boston: Artech House, 2001.
- [26] RAO S M. Electromagnetic scattering and radiation of arbitrary shape surfaces by triangular patch modeling[D]. Ph.D. Dissertation, Mississippi: Univ Mississippi, 1980: 1-20.
- [27] NIE Zai-ping, FANG Da-gang. Electromagnetic scattering characteristics of target and modeling, theory, method and implementation (elementary) [M]. Beijing: National Defense Industry Press, 2009a: 82-88 (in Chinese).
- [28] NIE Zai-ping, FANG Da-gang. Electromagnetic scattering characteristics of target and modeling, theory, method and implementation (advanced) [M]. Beijing: National Defense Industry Press, 2009b: 51-56 (in Chinese).

- [29] MAKAROV S. Antenna and EM modeling with MATLAB [M]. Princeton Univ Press, 2002: 10-40.
- [30] GALLAGHER M W, WHITEWAY J, FLYNN M J, et al. An overview of the microphysical structure of cirrus clouds observed during EMERALD-1 [J]. *J Roy Meteorol Soc*, 2004, 131: 1 143-1 169.
- [31] GANG Hong. Parameterization of scattering and absorption properties of nonspherical ice crystals at microwave frequencies [J]. *J Geophys Res*, 2007, 112: D11208.
- [32] AYDIN K, WALSH T M. Millimeter wave scattering from spatial and planar bullet rosettes [J]. *IEEE Trans Geosci Remot Sen*, 1999, 37 (2): 1 138-1 150.
- [33] ZHANG Pei-chang, DU Bing-yu, DAI Tie-pi. Radar Meteorolog, [M]. Beijing: China Meteorological Press, 2000: 145-165 (in Chinese).
- [34] TIAN L, HEYMSFIELD G M, HEYMSFIELD A J, et al. A study of cirrus ice particle size distribution using TC4 observations [J]. *J Atmos Sci*, 2010, 67(1): 195-216.
- [35] BAUM B A, HEYMSFIELD A J, YANG P, et al. Bulk scattering properties for the remote sensing of ice clouds. Part I: microphysical data and models [J]. *J Appl Meteorol*, 2005, 44: 1 885-1 895.
- [36] LIU C L, ILLINGWORTH A J. Toward more accurate retrievals of ice water content from radar measurements of clouds [J]. *J Appl Meteorol*, 2000, 39: 1 130-1 146.
- [37] MACE G G, HEYMSFIELD A J, POELLOT M R. On retrieving the microphysical properties of cirrus clouds using the moments of the millimeter-wavelength Doppler spectrum [J]. *J Geophys Res*, 2002, 107 (D24), 4815, doi:10.1029/2001JD001308.
- [38] SEO E K, LIU G . Retrievals of cloud ice water path by combining ground cloud radar and satellite high-frequency microwave measurements near the ARM SGP site [J]. *J Geophys Res*, 2005, 110, D14203, doi:10.1029/2004JD005727.
- [39] BROWN P R A, ILLINGWORTH A J, HEYMSFIELD A J, et al. The role of spaceborne millimeter-wave radar in the global monitoring of ice-cloud [J]. *J Appl Meteorol*, 1995, 34: 2 346-2 366.
- [40] AYDIN K, TANG C. Relationships between IWC and polarimetric radar measurements at 94 and 220 GHz for hexagonal columns and plates [J]. *J Atmos Ocean Tech*, 1997, 14 (5): 1 055-1 063.
- Citation:** WANG Jin-hu, GE Jun-xiang, WEI Ming et al. Study of the relationship between IWC and Z for nonspherical ice particles at millimeter wavelength [J]. *J Trop Meteorol*, 2016, 22(S1): 78-88.